

Electronic supplementary information (ESI)

Utilisation of *in situ* formed cyano-bridged coordination polymers as precursors of supported Ir–Ni alloy nanoparticles with precisely controlled compositions and sizes

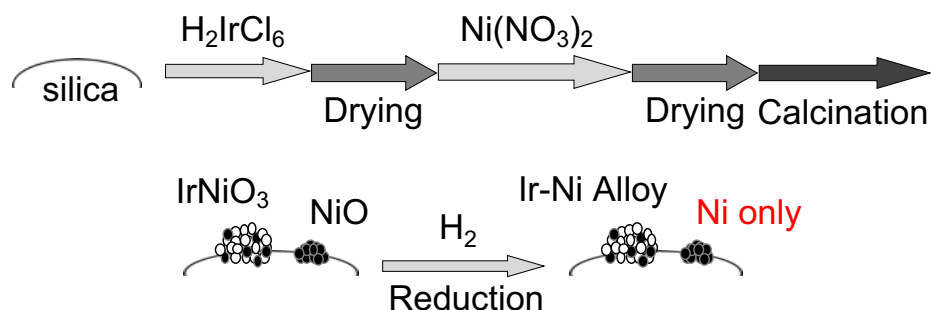
Yusuke Yamada,^{*ab} Miho Nishida,^a Tatsuya Nakabayashi,^a Takashi Nakazono,^b
Hanghao Lin,^a Pengru Chen,^a and Masazumi Tamura^{*ab}

^aDepartment of Chemistry and Bioengineering, Graduate School of Engineering, Osaka Metropolitan University, Sugimoto, Sumiyoshi, Osaka, 558-8585, Japan.

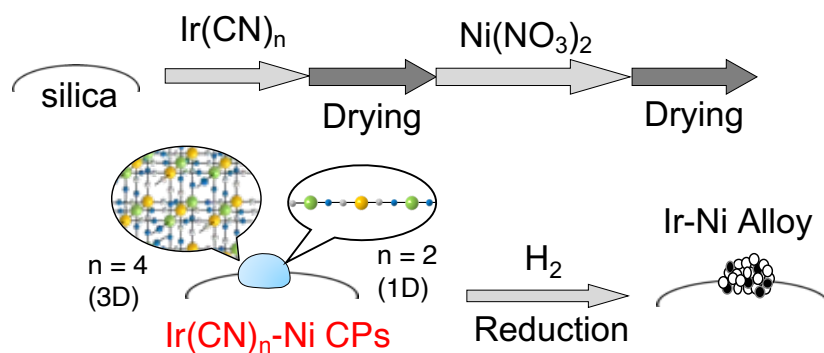
^bResearch Center for Artificial Photosynthesis, Osaka Metropolitan University, Sumiyoshi, Osaka 558-8585, Japan.

*E-mail: ymd@omu.ac.jp; mtamura@omu.ac.jp

a) Conventional method



b) This work



Scheme S1. Preparation methods of Ir-Ni alloys supported on SiO_2 by using $\text{Ni}(\text{NO}_3)_2$ and (a) H_2IrCl_6 and (b) $[\text{Ir}(\text{CN})_6]^{3-}$ (**$\text{Ir}(\text{CN})_6$**) or $[\text{Ir}(\text{ppy})_2(\text{CN})_2]^-$ (ppy = 2-phenylpyridine; **$\text{Ir}(\text{CN})_2$**) as precursors. Formation of unalloyed Ni nanoparticles (Ni only) is hardly avoidable with H_2IrCl_6 .

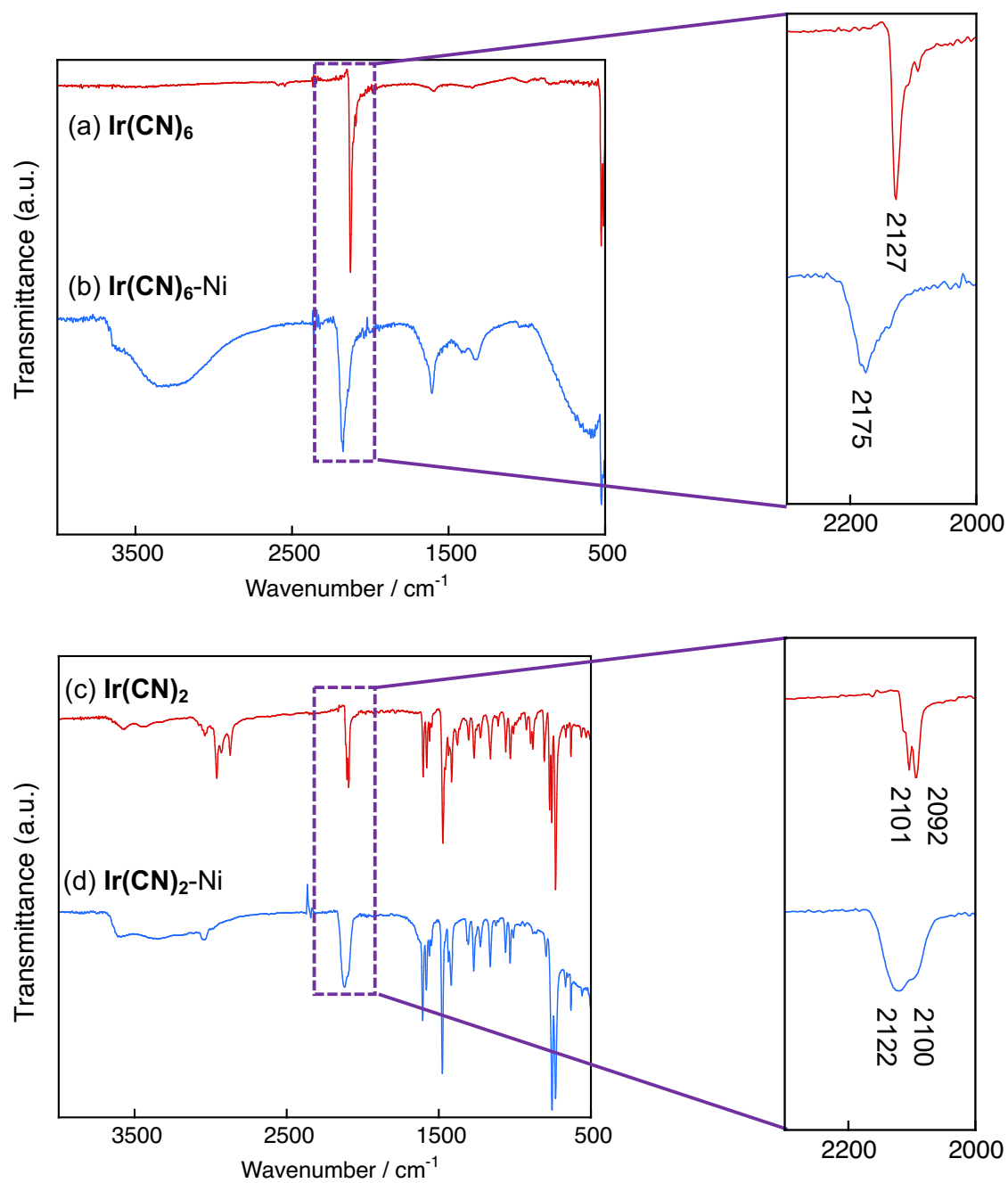


Fig. S1. IR spectra of (a) $\text{K}_3[\text{Ir}(\text{CN})_6]$ ($\text{Ir}(\text{CN})_6$), (b) $\text{Ni}_{1.5}[\text{Ir}(\text{CN})_6]$ ($\text{Ir}(\text{CN})_6\text{-Ni}$), (c) $(n\text{-Bu}_4\text{N})[\text{Ir}(\text{ppy})_2(\text{CN})_2]$ ($\text{Ir}(\text{CN})_2$) and (d) $\text{Ni}_{0.5}[\text{Ir}(\text{ppy})_2(\text{CN})_2]$ ($\text{Ir}(\text{CN})_2\text{-Ni}$).

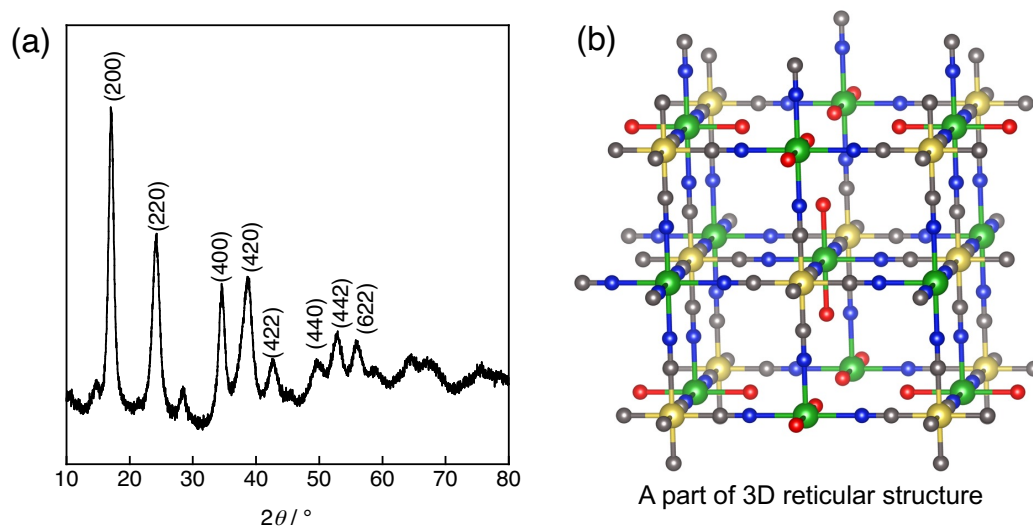


Fig. S2. (a) Powder X-ray diffraction pattern of $\text{Ni}_{1.5}[\text{Ir}(\text{CN})_6]$ ($\text{Ir}(\text{CN})_6\text{-Ni}$) and (b) a schematic drawing of the 3D reticular structure usually observed for Prussian blue analogues. The numbers in parenthesis are (hkl) indices.

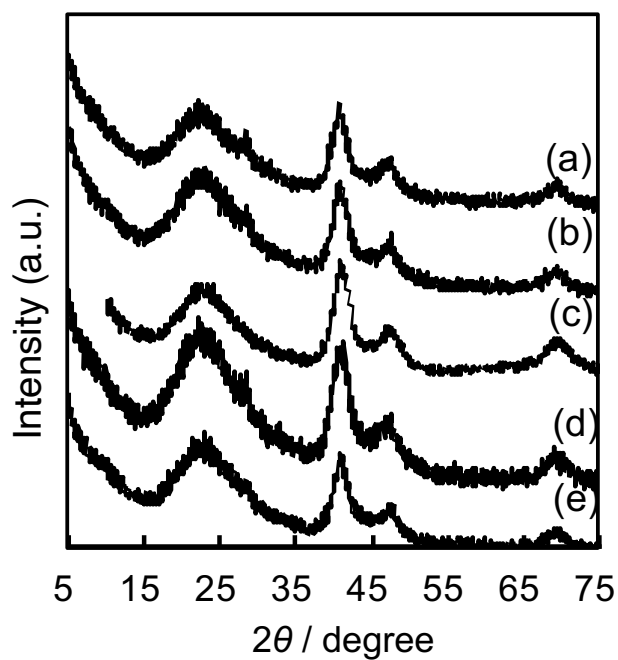


Fig. S3. Powder X-ray diffraction patterns of $\text{Ir}(\text{CN})_6\text{-Ni}/\text{SiO}_2\text{-X}$ [$X = \text{Ni}/(\text{Ni}+\text{Ir})$]. $X =$ (a) 0.05, (b) 0.10, (c) 0.15 (d) 0.20 and (e) 0.25 in wide range.

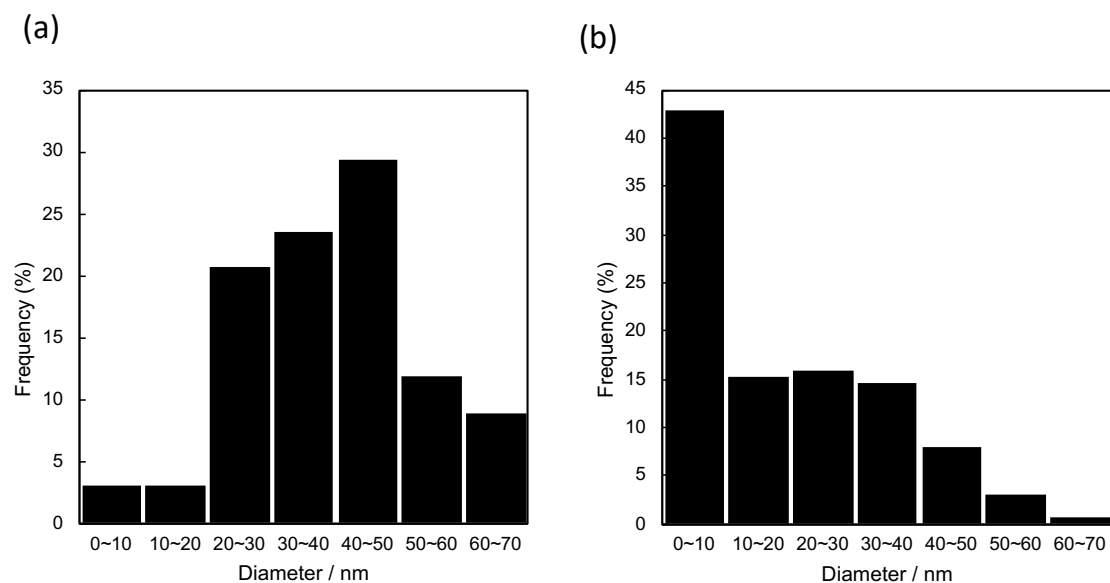


Fig. S4. Size distributions of supported particles in (a) $\text{Ir(CN)}_6\text{-Ni/SiO}_2\text{-0.2}$ and (b) $\text{Ir(CN)}_6\text{-Ni/SiO}_2\text{-0.4}$.

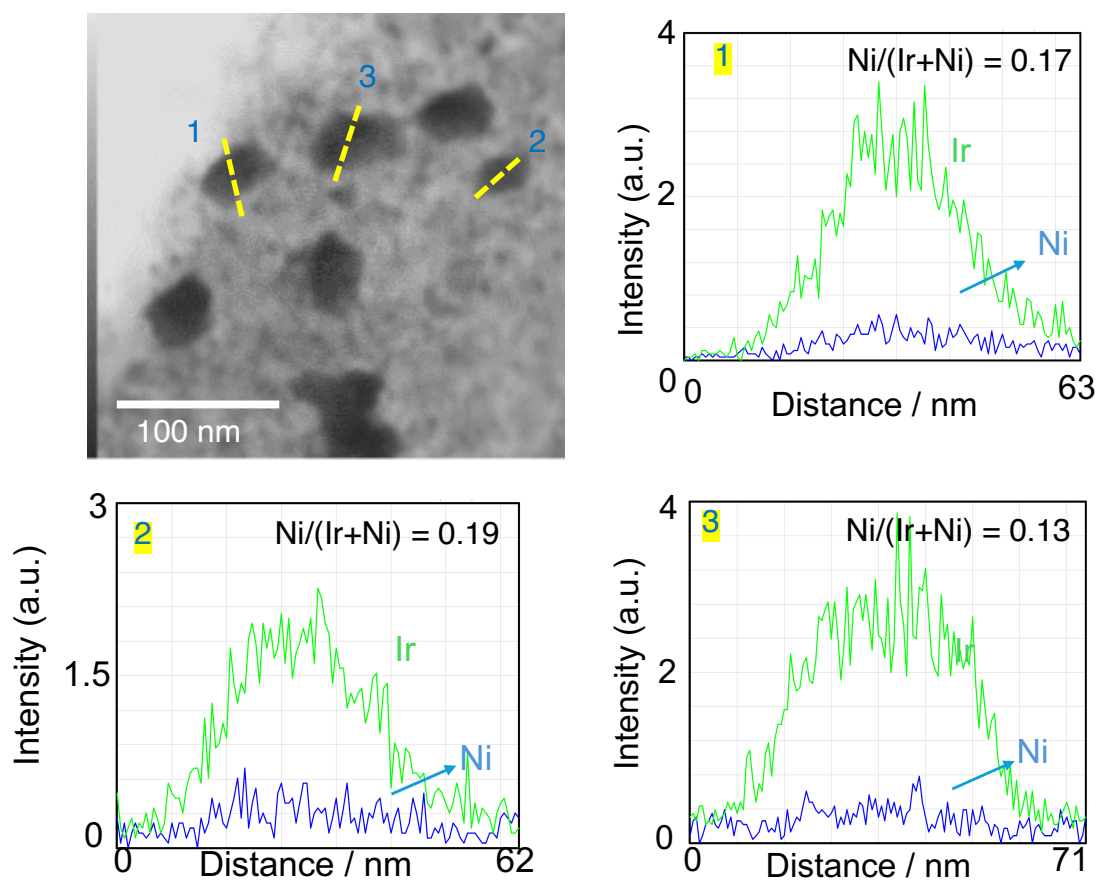


Fig. S5. EDX line scanning spectra of Ir and Ni of three single particles supported on SiO_2 ($\text{Ir(CN)}_6\text{-Ni/SiO}_2\text{-0.4}$).

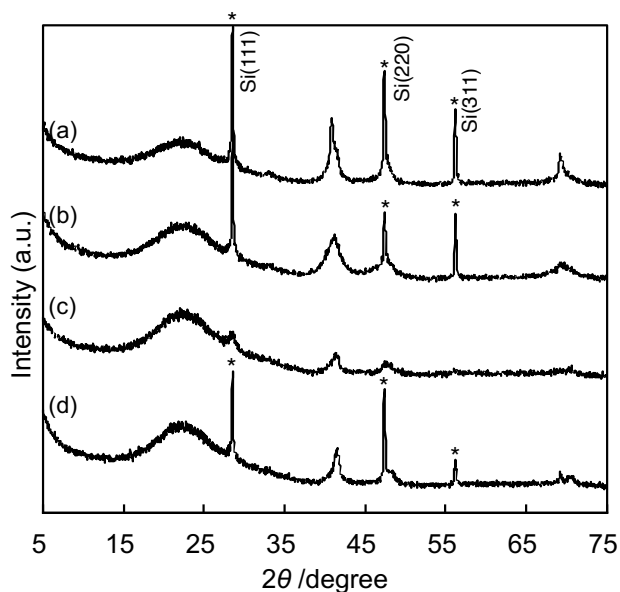


Fig. S6. PXRD patterns of (a) $\text{Ir(CN)}_2\text{-Ni/SiO}_2\text{-0.10}$, (b) $\text{Ir(CN)}_2\text{-Ni/SiO}_2\text{-0.15}$, (c) $\text{Ir(CN)}_2\text{-Ni/SiO}_2\text{-0.20}$ and (d) $\text{Ir(CN)}_2\text{-Ni/SiO}_2\text{-0.40}$. The peaks with * are ascribed to Si used as internal standard.

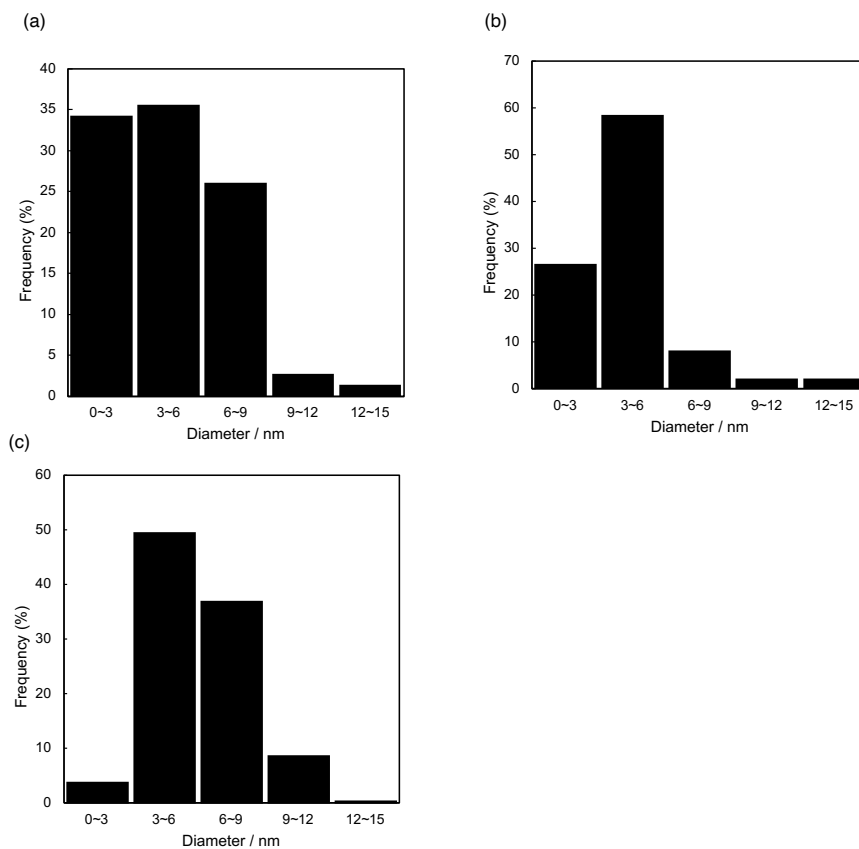


Fig. S7. Size distribution of supported particles of $\text{Ir(CN)}_2\text{-Ni/SiO}_2\text{-X}$. X = (a) 0.10, (b) 0.15 and (c) 0.40.

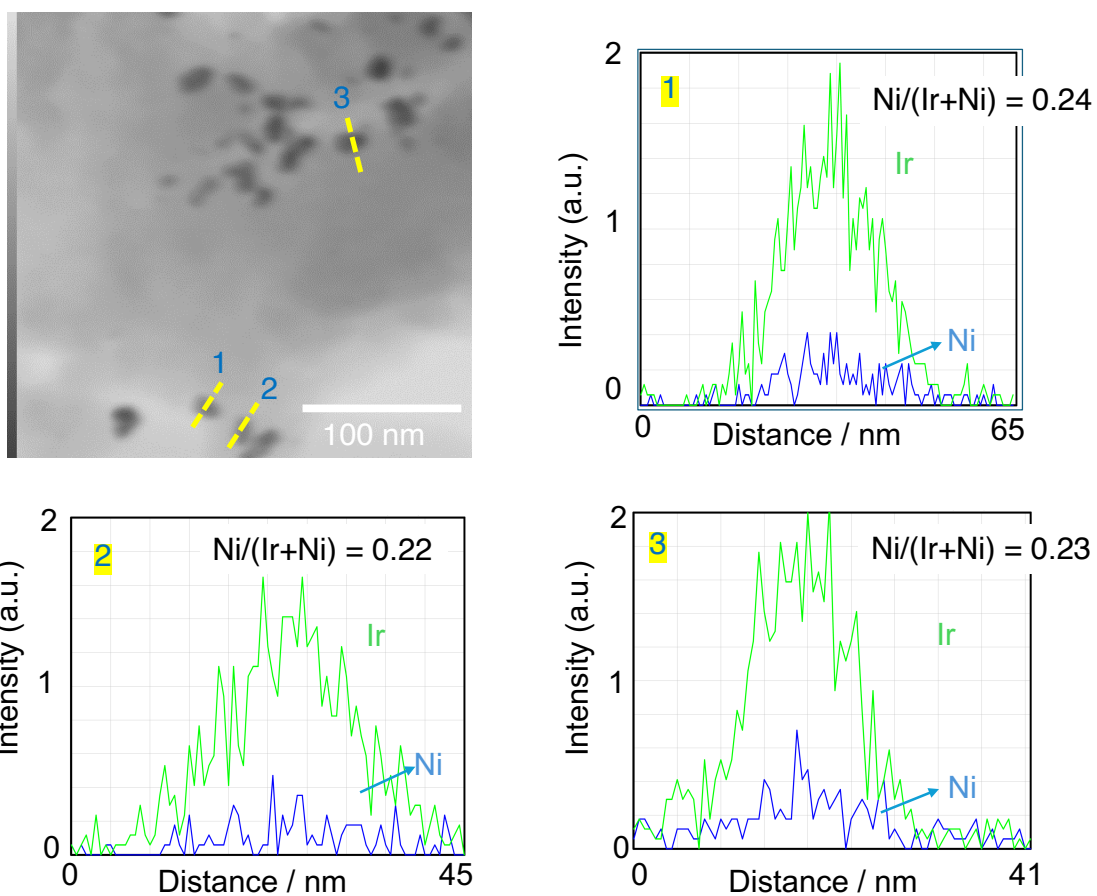


Fig. S8. EDX line scanning spectra of Ir and Ni of three single Ir-Ni particles supported on SiO_2 ($\text{Ir}(\text{CN})_2\text{-Ni/SiO}_2\text{-0.4}$).

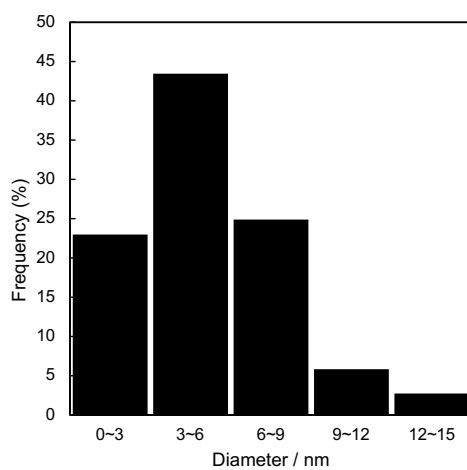


Fig. S9. Size distribution of supported particles of $\text{Ir}(\text{CN})_2\text{-Ni/SiO}_2\text{-Al}_2\text{O}_3\text{-0.2}$.